Journal of Advanced Research in Fluid Mechanics and Thermal Sciences

Journal homepage:
https://semarakilmu.com.my/journals/index.php/fluid_mechanics_thermal_sciences/index
ISSN: 2289-7879

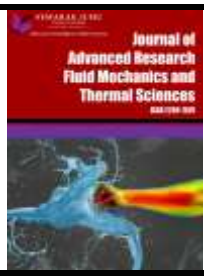

Fluid-Structure Interaction Modelling of Blood Flow in Peripheral Arterial Disease

Muhammad Firdaus Mohd Fauzi[1], Nasrul Hadi Johari[1,2,*], Mohd Jamil Mohamed Mokhtarudin[3], Bazli Mohd Yusoff[4], Baolei Guo[5]

[1] Faculty of Mechanical and Automotive Engineering Technology, Universiti Malaysia Pahang Al-Sultan Abdullah, 26600 Pekan, Pahang, Malaysia
[2] Centre for Advanced Industrial Technology, Universiti Malaysia Pahang Al-Sultan Abdullah, 26600 Pekan, Pahang, Malaysia
[3] Faculty of Manufacturing and Mechatronics Engineering Technology, Universiti Malaysia Pahang Al-Sultan Abdullah, 26600 Pekan, Pahang, Malaysia
[4] Department of Radiology, School of Medical Sciences, Universiti Sains Malaysia, Kubang Kerian, 16150 Kota Bharu, Kelantan, Malaysia
[5] Department of Vascular Surgery, Institute of Vascular Surgery, Zhongshan Hospital, Fudan University, Shanghai, China

ARTICLE INFO

Article history:
Received 27 February 2024
Received in revised form 15 June 2024
Accepted 24 June 2024
Available online 15 July 2024

Keywords:
Peripheral arterial disease; fluid-structure interaction; atherosclerosis; hemodynamics

ABSTRACT

The study presents the fluid-structure interaction (FSI) modeling in Peripheral Arterial Disease (PAD) geometry, highlighting the effects of arterial blockage on hemodynamics and arterial wall mechanics. Employing a RANS-based SST-Tran model, the study examines stenotic PAD models under realistic boundary conditions, coupled with a hyperelastic Mooney-Rivlin model to simulate the arterial wall's response. The analysis includes velocity profiles, wall shear stress (WSS), pressure distribution, and wall displacement, revealing significant differences between healthy and stenosed models. It demonstrates adaptive hemodynamics, the impact of stenosis on flow mechanics, and potential implications for atherosclerosis and plaque formation. The findings highlight the importance of understanding stenosis severity for clinical risk assessment, treatment planning, and monitoring.

1. Introduction

The PAD occurs when blood vessels in the legs narrow or become blocked, leading to reduced blood flow to the legs and feet. This restriction of blood flow is a manifestation of cardiovascular disease (CVD), elevating the risk of heart attacks and strokes for patient [1]. In 2010, approximately 202.06 million people were affected by PAD, with a subsequent 17% increase over five years, reaching 236 million in 2015 [2]. Atherosclerosis, characterized by the thickening and hardening of arterial walls due to plaque buildup, further impedes blood flow to the legs and feet, heightening the risk of cardiovascular events such as heart attacks and strokes [3].

To comprehend the mechanisms of PAD, the study of blood hemodynamics is crucial. Local changes in wall shear stress (WSS) in stenosed areas are correlated with PAD development, as

* *Corresponding author.*
E-mail address: nhadi@umpsa.edu.my

https://doi.org/10.37934/arfmts.119.1.117133

atheroma tends to form in regions exposed to low WSS. Numerous studies indicate that the risk of PAD development is linked to WSS and blood flow characteristics [4]. Researchers have employed Computational Fluid Dynamics (CFD) to simulate and analyze hemodynamic parameters in complex stenotic peripheral artery areas, with reported consistency between WSS measurements in CFD and those obtained through Magnetic Resonance Imaging (MRI) [5-8].

However, CFD analysis has limitations, particularly in illustrating the artery wall, as it considers only blood behaviour and treats the arterial wall as a rigid structure. To address this limitation, FSI modelling becomes valuable [8]. FSI incorporates both blood flow and arterial wall dynamics by assuming the deformability of the arterial wall [9,10]. This approach allows for bidirectional feedback between blood flow and the arterial wall, offering insights into how flow influences wall response and how wall deformation affects blood flow [11]. To illustrate atherosclerosis, FSI modelling has been applied to predict WSS and the distribution of low-density lipoproteins (LDL) within arterial walls [12]. Javadzadegan *et al.,* [13] used FSI modelling to examine the effect of physiological waveforms on peripheral arteries to observe local thrombus in the region. Wang *et al.,* [14] later improvised the FSI model by using patient-specific models in order to observe the hemodynamic performance and its interaction with the peripheral arterial wall that may cause atherosclerosis development. Earlier, Kim *et al.,* [15] introduced the usage of FSI modelling in human femoral bifurcation to investigate the influence of wall motion on the hemodynamic parameters. However, none of the previous FSI studies in PAD focus on comparing and validating the computational predictions with the clinical follow-up data. Gökgöl *et al.,* [16] have directly involved the high-resolution optical coherence tomography (OCT) images compared to their CFD predictions; however, the femoral arterial wall was negligible.

While previous FSI studies in PAD have explored various aspects, including physiological waveforms, patient-specific models, and wall motion in the femoral bifurcation, there needs to be a greater focus on the impact of varying degrees of artery blockage in PAD. Therefore, this research project aims to develop an FSI model to predict potential atherosclerosis locations in healthy and stenosed peripheral arteries, precisely at 70% and 90% stenosis levels. These studies will provide valuable insights into the complexities of hemodynamics and arterial wall mechanics. Specifically, there remains a need to address the influence of the percentage of artery blockage on blood flow patterns and wall deformations. Understanding how different levels of stenosis affect the fluid-structure interaction in peripheral arteries.

2. Methodology

2.1 Geometry Construction and Meshing

In this study, we developed an idealized model of common femoral artery featuring two branches: superficial femoral artery and profunda femoral artery. The dimensions of the geometry, including diameter, curvature, and wall thickness, were determined based on clinical data available in Table 1 [13,17-19]. The geometry construction was executed using Solidworks 2022 (Dassault Systems, Velizy, France).

Table 1
Geometric parameters [13]

Segment	Measurement
Diameter CFA and SFA	6.7 mm
Diameter PFA	6.0 mm
Length CFA	30 mm
Length SFA	100 mm
Length PFA	100 mm
Wall thickness CFA and SFA	0.92 mm
Wall thickness PFA	0.82 mm
Branching angle, α	45°

The model was divided into two distinct parts: the solid domain, representing the arterial wall, and the fluid domain, representing the blood flow. Figure 1 illustrates the initial creation of the fluid domain. Subsequently, the solid domain was formed using shell features, ensuring proper surface finishing at the bifurcation.

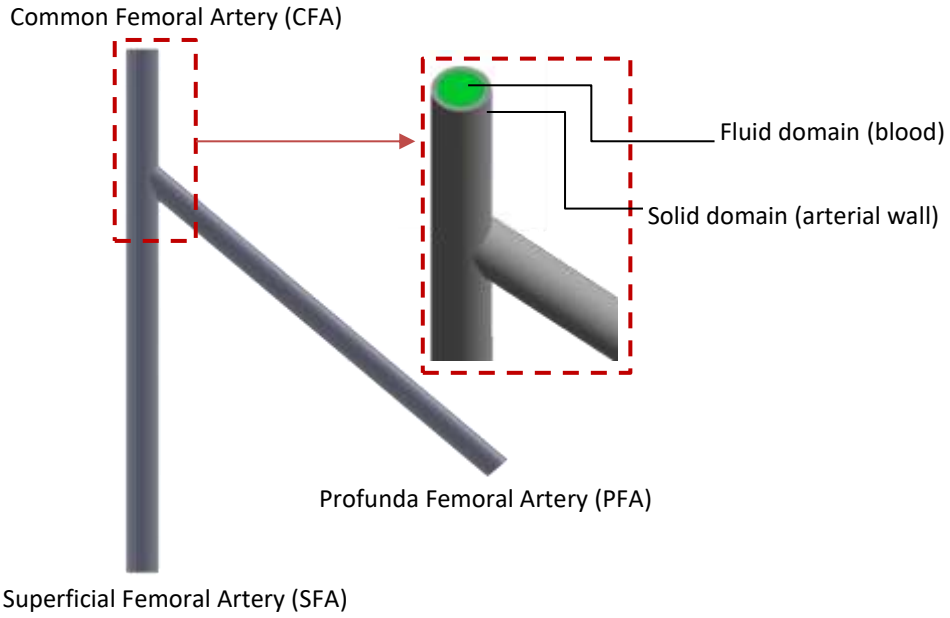

Fig. 1. Idealised femoral artery geometry, and the solid and fluid domain for FSI simulation

This study used the trapezium-type stenosis model shown in Figure 2, a configuration frequently utilized in clinical studies involving patient cohorts [20,21]. Consequently, the research will concentrate on assessing stenosis severity levels, specifically targeting moderate (70%) and severe (90%) stenosis conditions at the superficial femoral artery. This selection is based on the established relevance of these degrees of stenosis in clinical investigations, ensuring a meaningful and clinically representative examination of the chosen stenotic conditions [22-24].

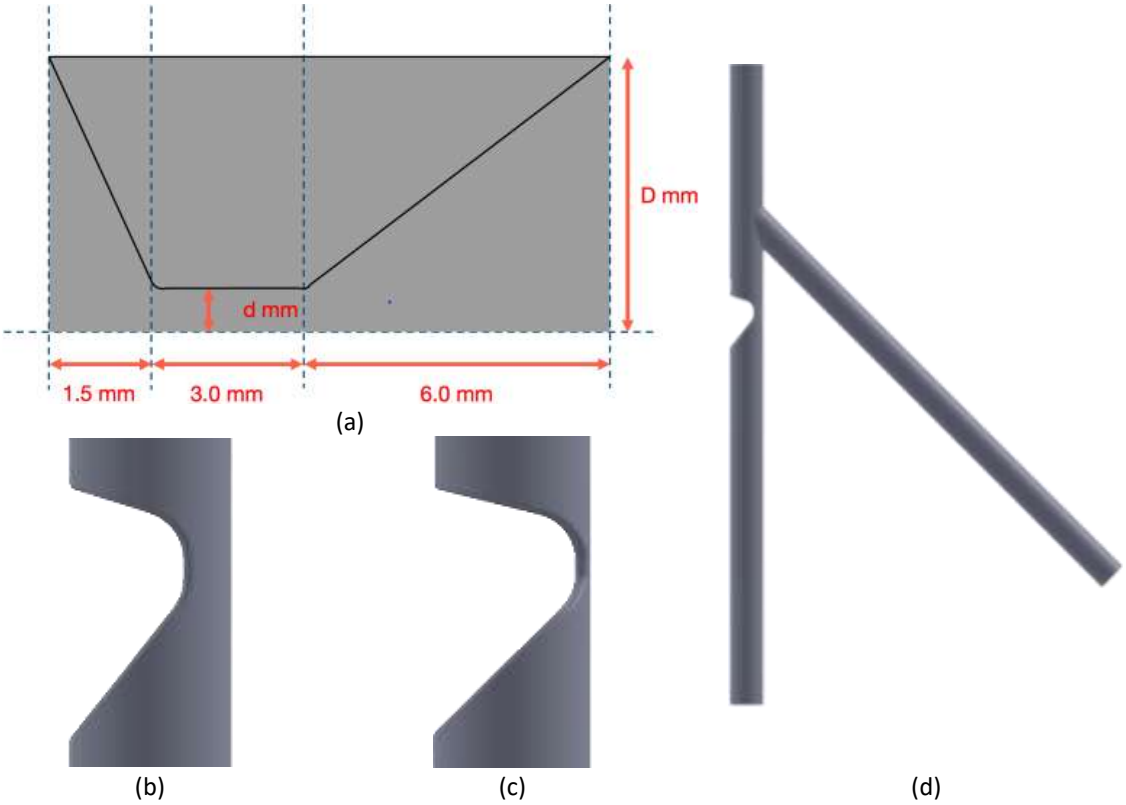

Fig. 2. (a) Stenosis schematic diagram for idealised stenosed, (b) 70% of blockage, (c) 90% of blockage, and (d) Idealised peripheral artery with stenosis

The idealised peripheral artery geometry was saved in the Parasolid format and exported to ANSYS workbench (ANSYS Inc, Canonsburg, PA, USA) for mesh construction and CFD simulation. The geometry was discretized into unstructured mesh with 3D tetrahedral cells for the entire geometry. To ensure the mesh quality, the elements were verified for attributes such as element quality, skewness, and orthogonal quality [25]. Acceptable standards were set, with a minimum orthogonal quality of 0.15 or higher being acceptable, and a maximum skewness of less than 0.94 being considered acceptable [26]. A mesh independence test was conducted on three different mesh size models. The study revealed negligible flow velocity variations across all three employed meshes. However, the WSS varied by more than 5% when comparing the 1.25 x 10^7 elements mesh to the course 7 x 10^6 elements mesh, but less than 2% when compared to a finer mesh of 2 x 10^7 elements. Consequently, the intermediate 1.25 x 10^7 elements mesh exhibited practical independence, implying that additional mesh refinement was chosen for the simulations. Optimal grid resolution near the vessel walls was ensured by maintaining the maximum height of wall cells, in wall units (y+), at approximately 1, with an average value below 0.5.

2.2 Boundary Conditions

Within the fluid domain, blood viscosity plays a crucial role in influencing the dynamics of blood flow within vessels [24]. For the purposes of this FSI simulation, blood behaviour was simplified to a Newtonian fluid [27]. In reality, a non-Newtonian fluid, especially in the context of smaller vessels such as capillaries, whilst larger vessels like the carotid, aortic segments, and peripheral arteries are commonly treated as Newtonian fluids in simulations [14,24]. In this study, blood was assumed to be a Newtonian fluid with a density of 1060 kg/m³ and a viscosity of 0.0035 kg/(m·s) [5,14,24].

The blood flow was considered to exhibit a steady laminar pattern, characterized by a Reynolds number (Re) of 1260. The chosen inlet velocity corresponded to the accelerated flow condition, just prior to peak systole (as depicted in Figure 3). This selection was aligned with the typical flow patterns observed in healthy peripheral blood vessels, such as the femoral artery, where laminar flow and corresponding Reynolds numbers were commonly encountered, as detailed in previous studies [10,12]. For the stenotic model, the study employed the RANS-based SST-Tran model, merging aa $k-\omega$ model within the boundary layer's inner region with a $k-\epsilon$ model in the outer region and free shear flows [28,29]. This model also incorporated a transitional model with two additional transport equations, which were formulated locally for intermittency and the transition onset criterion, based on the momentum thickness Reynolds number. Featuring advanced correlations for transition, this model had been applied to a broad spectrum of engineering problems, including turbomachinery [28,30,31], aircraft configurations, wind turbines, and was noted for its promising results in cardiovascular flow applications [32]. To simulate physiologically realistic transitional flow, the turbulence intensity level was set at the inlet. Defined as the ratio of the turbulent velocity fluctuations' root mean square to the mean velocity, the turbulence intensity (Tu) was established at 5% for the inlet conditions in the SST-Transition simulations, drawing on the findings from previous research [33]. The simulation assumptions included rigid walls with no-slip conditions, ensuring that all velocity components at the wall were zero. The model was available in ANSYS CFX 2021, and the numerical solution was achieved using an additive correction strategy alongside a coupled algebraic multigrid approach, reaching close to second-order accuracy, following the methodology established by Hutchinson and Raithby [34].

The pressure values at the outlets of the SFA and the PFA were set using precise velocity and pressure waveforms derived from human femoral artery blood flow studies, as referenced from Kim *et al.,* [15] and Colombo *et al.,* [35] and illustrated in Figure 3. These boundary conditions are critical for accurately representing physiological blood flow conditions and ensuring the relevance of the simulation outcomes to real-world scenarios.

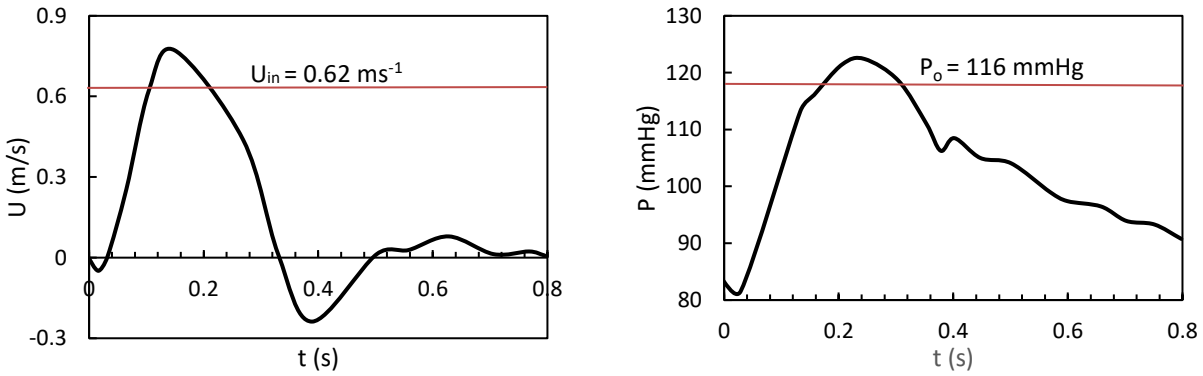

Fig. 3. (a) Velocity waveform, and (b) pressure waveform of blood flow in human femoral artery. The inlet velocity (U_{in}) and pressure outlet (P_o) is based on a specific value to represent steady flow simulation

For the solid domain, the arterial wall was modeled with a realistic elastic behavior, incorporating hyperelastic model to enhance the precision of simulation outcomes. Specifically, the Mooney-Rivlin hyperelastic model with five parameters was employed to accurately capture the material's response, as detailed in Table 2 [36]. Fixed support features were implemented at the ends of the inlet and outlets to allow appropriate wall displacement, effectively restraining the solid structure and mimicking its fixed behavior.

The fluid forces derived from CFD results were imported and applied to the inner femoral arterial wall within ANSYS Structural. This approach facilitated an accurate representation of the fluid forces acting on the arterial wall, enabling a comprehensive study of fluid-structure interaction within the system. The utilization of hyperelastic models and the incorporation of realistic boundary conditions enhance the fidelity of the simulation, contributing to more meaningful insights into the complex dynamics of blood flow and its interaction with the arterial wall.

Table 2
Five parameters of Mooney Rivlin [36,37]

Model	Equation	Parameters
Mooney-Rivlin	$\sigma = C_{10}(I_1 - 3) + C_{01}(I_2 - 3) + C_{20}(I_1 - 3)^2 + C_{11}(I_1 - 3)(I_2 - 3) + C_{02}(I_1 - 3)^2$	$C_{10} = 18.9\ kPa$, $C_{01} = 2.75\ kPa$, $C_{20} = 590.42\ kPa$, $C_{11} = 857.18\ kPa$, $C_{02} = 0\ kPa$

2.3 Fluid-structure Interaction Simulation

Although the current study does not involve fully coupled FSI, it presents an initial exploration of the impact of fluid forces on the arterial wall. This was achieved through the direct coupling of fluid forces, solved by the finite volume model ANSYS Fluent, applied to the inner wall of the structural domain. The fluid dynamics are governed by the Navier-Stokes equations for incompressible flow, which can be expressed as:

$$\nabla \cdot \mathbf{v} = \mathbf{0} \tag{1}$$

$$\rho\left(\frac{\partial \mathbf{v}}{\partial t} + \mathbf{v} \cdot \nabla . \mathbf{v}\right) = -\nabla . p + \mu \nabla^2 \mathbf{v} + \mathbf{f} \tag{2}$$

where **v** is the velocity field, ρ is the fluid density, p is the pressure, μ is the dynamic viscosity, and **f** represents body forces. The structural response to the fluid forces is modeled using the equations of the Mooney-Rivlin model for hyperelastic materials.

$$\nabla \cdot \sigma + \mathbf{f}_{\text{body}} = \rho_s \frac{\partial^2 \text{u}}{\partial t^2} \tag{3}$$

Here, σ is the stress sensor, $\mathbf{f}_{\text{body}}$ are body forces acting on the structure, ρ_s is the density of the structural material, and $\frac{\partial^2 \text{u}}{\partial t^2}$ represents the acceleration of the material points in the structure.

The stress σ in a hyperelastic material described by the 5-parameter Mooney-Rivlin model is given by the equation in Table 2.

For wall stress simulation, a finite element-based software, ANSYS Structural, was employed. The FSI simulations were executed on a desktop with an Intel(R) Core (TM) i7-4790S CPU @ 3.20GHz, 16GB RAM, and a 1TB HDD. While not fully coupled, this approach allows for an initial examination of the influence of fluid flow on the arterial wall, providing valuable insights into the preliminary aspects of fluid-structure interaction in the context of peripheral arterial dynamics.

3. Results and Discussion

3.1 Velocity Contours

Figure 4 illustrates the velocity distribution across cross-sectional areas along the vessels of the idealized healthy and stenosed peripheral artery. Figure 4(a) shows the flow velocity exhibits a progressive increase along CFA toward the branching of SFA and PFA, reaching a peak velocity of 0.87 m/s just before the branching. Subsequently, the flow gradually decreases as it passes the bifurcation junction, with a simultaneous marginal skewing towards the apex of the bifurcation. A notable observation is the presence of a large flow recirculation zone with low-magnitude velocities in the outer wall of the PFA. This recirculation zone is initially recorded in the outer wall of PFA before stabilizing towards the outlet. Additionally, a recirculation zone is observed in the outer wall area of the SFA. It is noteworthy that normal peak systolic velocity values in the femoral artery typically fall within the range of approximately 0.45 m/s to 1.80 m/s [38]. These values serve as a reference range for assessing the health and functionality of the femoral artery in clinical settings. It is essential to recognize that the velocity of blood flow in the femoral artery can vary based on various factors, including the individual patient's characteristics, their health status, and the specific location within the artery under consideration [19].

In Figure 4(b) and Figure 4(c), depicting arteries with stenoses of 70% and 90%, a consistent pattern emerges. In both instances, there is a notable peak velocity at the site of stenosis, although the consequences become more pronounced with increasing severity of stenosis. In Figure 4(b), representing a 70% stenosed artery, a distinct peak velocity is observed within the stenosed region. Beyond the stenosis, there is a substantial reduction in flow, resulting in a significantly diminished flow rate. The presence of a sizable flow recirculation zone with low-magnitude velocities is noted along the wall of the SFA both before and after the stenosis, as well as on the outer wall of PFA. Notably, the recirculation zone recorded after the stenosis in the PFA shows stabilization toward the outlet.

Moving to Figure 4(c), depicting a 90% stenosed artery, a similar pattern emerges with a peak velocity at the stenosed area. However, in this case, the flow experiences a substantial decrease, eventually reaching zero, indicating a near-total blockage. This aligns with the concept of critical stenosis, where severe narrowing results in a significant impediment to blood flow, approaching complete obstruction. The observed flow patterns in both scenarios provide a nuanced understanding of how varying degrees of stenosis impact blood flow dynamics.

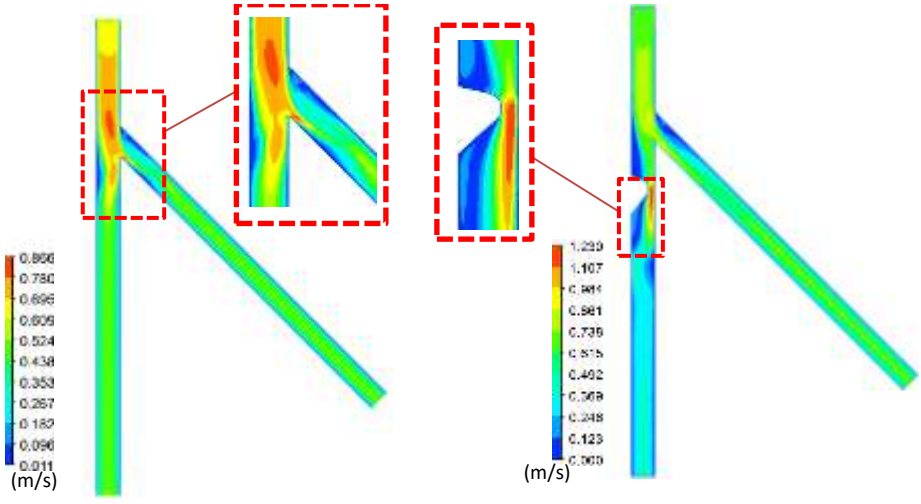

(a) (b)

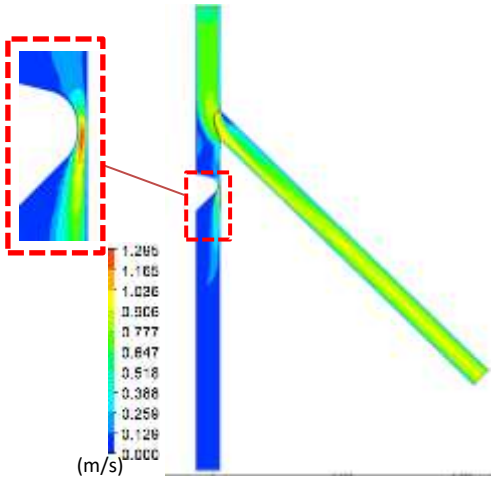

(c)

Fig. 4. Velocity contours (m/s) (a) normal artery, (b) 70% blockage, and (c) 90% blockage

Figure 5 shows the maximum outlet velocity in normal artery, artery with stenosed 70% and 90%. In the normal artery, the Outlet SFA velocity is 0.73 m/s, which is higher than the Outlet PFA velocity of 0.39 m/s. This suggests a typical hemodynamic profile in a healthy arterial system, with blood flow exhibiting expected patterns and velocities within physiological ranges.

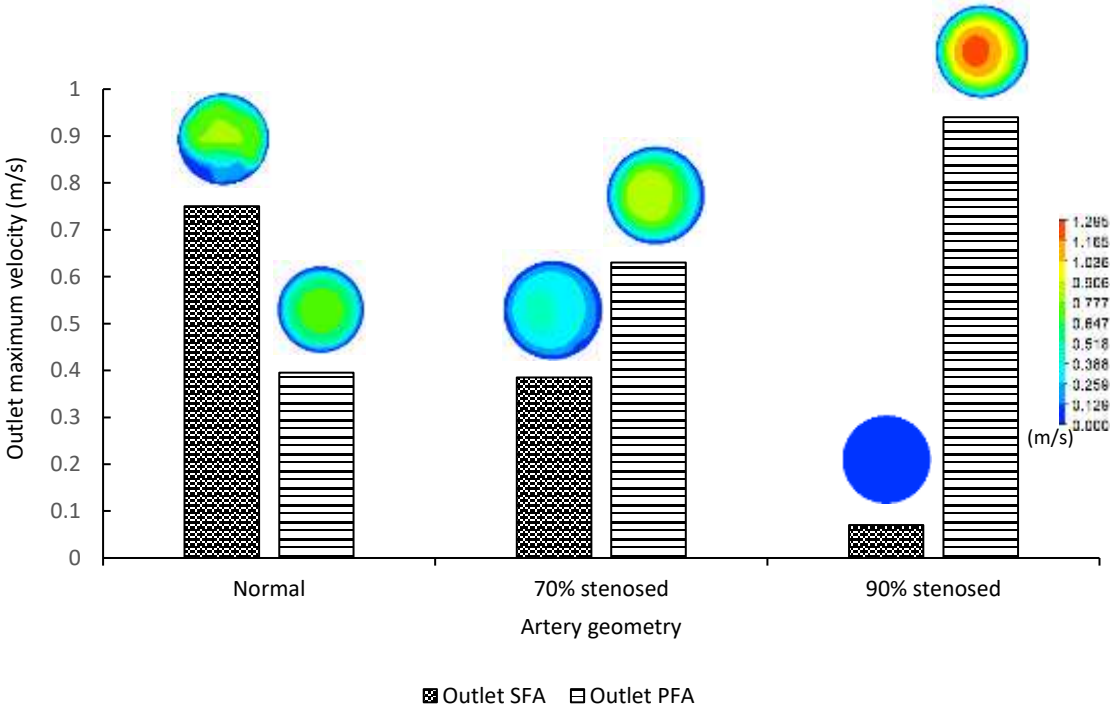

Fig. 5. Maximum outlet velocity at SFA and PFA in all peripheral artery models. The maximum velocity is shifting from SFA in normal model into PFA in stenotic models

Moving to the artery with a 70% blockage at the SFA, there is a noticeable reduction in Outlet SFA velocity (0.38 m/s) compared to the normal artery. In contrast, the Outlet PFA velocity has increased to 0.64 m/s. This shift in velocities may indicate adaptive hemodynamics in response to the partial blockage, with altered flow distribution between the SFA and PFA.

In the case of a 90% blockage at the SFA, there is a substantial decrease in Outlet SFA velocity (0.06 m/s), signifying severe restriction of blood flow. However, the Outlet PFA velocity has significantly increased to 0.97 m/s. This marked increase in PFA velocity suggests a compensatory mechanism to maintain overall blood flow in the presence of critical stenosis in the SFA.

Comparing velocities across conditions reveals a clear trend of decreasing SFA velocities with increasing stenosis severity (Normal > 70% Blockage > 90% Blockage). The reduction in SFA velocities is most pronounced in the 90% blockage condition, highlighting the critical impact on blood flow. Additionally, PFA velocities increase with increasing SFA blockage, emphasizing the compensatory role of collateral circulation, with the highest PFA velocity observed in the 90% blockage condition.

Physiologically, these results have significant implications. The normal artery velocities represent baseline hemodynamic values, while the altered velocities in stenosed conditions indicate compromised blood flow. Clinically, these findings can aid in risk assessment, treatment planning, and monitoring the progression of arterial diseases.

3.2 Wall Shear Stress Contours

WSS characterizes the force applied by the circulating blood on the endothelial cells lining the inner surface of an artery [39]. In Figure 6, the WSS contours for both healthy and stenosed arteries are depicted, with contours set to a maximum of 0.4, represented by red contours. Regions surpassing 0.4 WSS are highlighted in red, considering that a WSS value lower than 0.4 Pa is widely recognized as a potential contributor to atherosclerosis development [39,40].

Examining Figure 6(a), where WSS contours are derived from CFD simulations, a notable impact on flow behaviors is revealed. The bifurcation junction exhibits improper flow distribution and altered flow directions, leading to significant disparities in WSS. Throughout the artery's geometry, WSS consistently remains above 0.4 Pa. However, at the bifurcation site, where blood flow diverges into two branches, a change in flow direction occurs, contributing to increased complexity in the flow pattern. Importantly, Figure 6(a) identifies regions of low WSS after the bifurcation at the SFA and PFA, suggesting a heightened susceptibility to plaque formation in these areas.

In Figure 6(b), which represents a 70% stenosed artery, the analysis reveals notable occurrences of low WSS, particularly evident in regions encompassing the SFA and the outer section of the PFA. However, a significant observation lies in the extensive low WSS area around the stenosed region.

Moving to Figure 6(c) is artery with a 90% stenosed, a distinct pattern emerges. Notably, along the SFA, the WSS is observed to be exceptionally low, almost approaching zero. This phenomenon is closely tied to the nearly stagnant velocity of blood flow in the severely stenosed region.

The drastic reduction in WSS along the SFA is primarily attributed to the critical stenosis, where the arterial lumen is significantly narrowed, impeding the flow of blood. As the blood encounters the severe constriction, the velocity diminishes substantially, leading to an almost negligible WSS along this portion of the artery.

This observation aligns with the concept of critical stenosis, where the severity of arterial narrowing reaches a point that blood flow is severely hindered, approaching complete obstruction. The near-zero WSS along the SFA in the 90% stenosed artery underscores the critical nature of this stenotic condition and highlights the potential for adverse clinical outcomes, emphasizing the importance of understanding these hemodynamic changes in the context of arterial health.

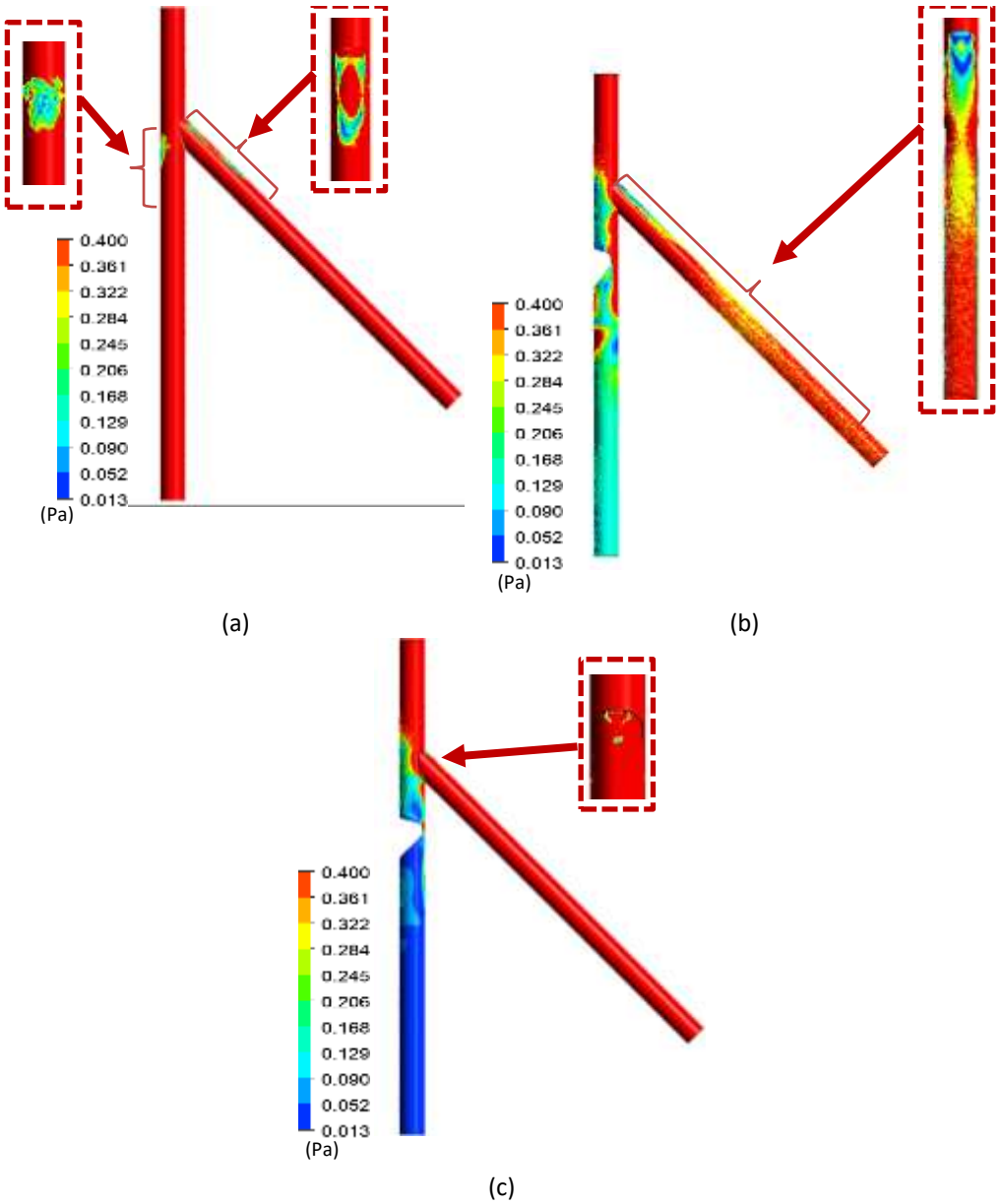

Fig. 6. WSS contours (Pa) in (a) normal artery, (b) 70% blockage, and (c) 90% blockage

3.3 Pressure

Figure 7 is pressure measurements obtained along the length of normal and stenosed femoral artery models. All three arteries show an initial increase in pressure which is attributed to the bifurcation. In the normal artery, pressure declines linearly which represents uniform losses from viscous shear along the length. With introduction of stenosis, markedly different profiles emerge. Localized pressure depressions are visible through the stenosed zones, with drops below the surrounding baseline for the respective cases. This corresponds to acceleration through the tighter stenosis and elevated friction within the lesion.

Notably, recordings also exhibit slight recoveries in 70% and 90% stenosed immediately post-stenotic before exhibiting re-decline. As elucidated, this unexpected finding results from transitional deceleration into the widening artery, converting fluid kinetic energy temporarily back into static pressure. However, irrecoverable dissipation resumes further downstream, preventing full return to inlet levels.

The complex pressure landscape illustrates fluid behavior through an idealized stenosis, marked by inertial losses, turbulence production, and minor proximal overshoots. Discrepancies from normal trace to fundamental alterations in flow mechanics imposed by the narrowed geometry. Quantification enables models examining stenosis progression or surgical planning to improve patient outcomes.

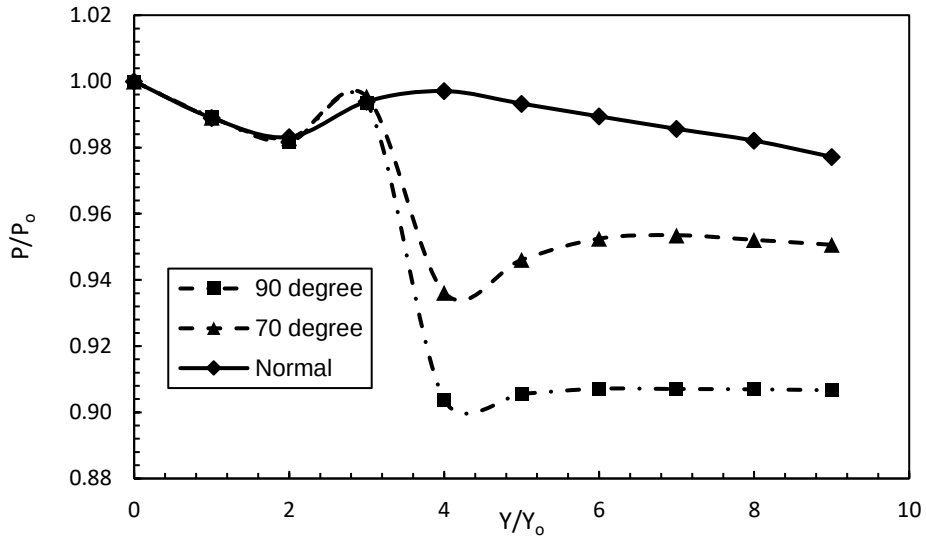

Fig. 7. Normalized pressure along Y axis

3.4 Wall Displacement

The quantitative assessment of total deformation in the arterial geometries shows in Figure 8 reveals a notable trend of increasing deformation with higher degrees of stenosis. In the normal artery, the total deformation is recorded at 0.21 mm, indicating the baseline structural response under healthy conditions. Transitioning to a 70% stenosed artery, there is a substantial increase in deformation, with the value reaching 0.95 mm. This jump in deformation highlights the significant impact of moderate stenosis on arterial structure, showcasing the structural alterations induced by the narrowing of the artery.

The trend further intensifies in the presence of 90% stenosis, where the total deformation reaches 1.87 mm. This drastic increase in deformation aligns with the concept of critical stenosis, where the arterial geometry experiences severe narrowing, resulting in a concentrated and localized impact on fluid dynamics and wall stresses. The observed trend underscores the progressive influence of stenosis severity on arterial deformation.

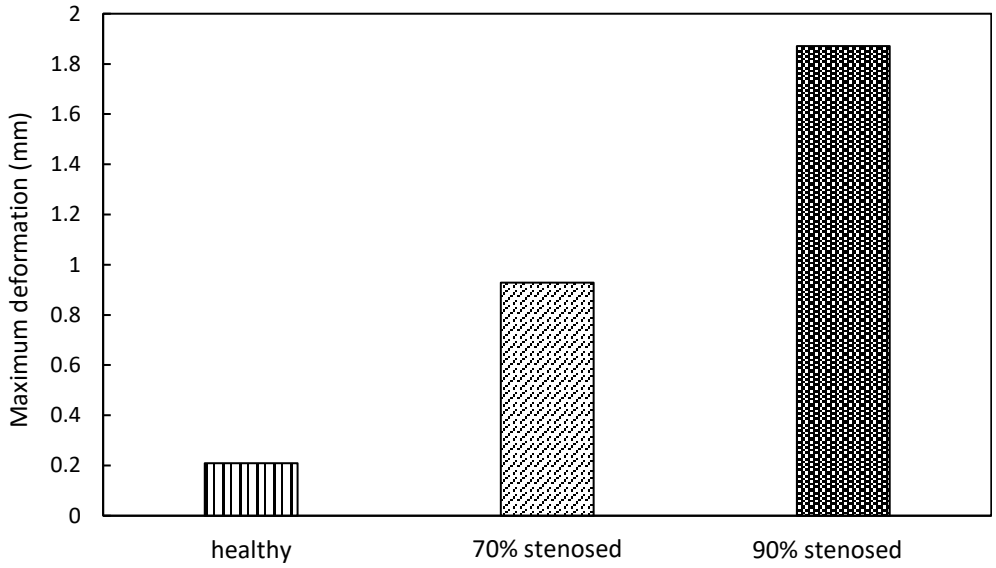

Fig. 8. Maximum deformation

Figure 9 are the deformation of the healthy and stenosed idealized geometry. Figure 9(a) shows the maximum deformation occurs after the bifurcation, primarily due to the changes in arterial geometry causing the flow separation into the branches producing higher fluid forces to the wall. This heightened deformation in the region after bifurcation makes it susceptible to plaque formation area and possible for rupture [41]. This heightened deformation subsequent to the bifurcation holds significant implications for the stress levels within the artery. Elevated stress levels can potentially contribute to plaque rupture, a phenomenon that has been noted by Tang *et al.,* [42] who reported that 82% of plaque fractures occurred in regions characterized by high stress.

Figure 9(b) and Figure 9(c) reveal that the maximum deformation occurs at the stenosed area, a phenomenon attributed to the narrowing of the artery due to stenosis [43,44]. This constriction alters blood flow dynamics, inducing higher fluid forces on the arterial wall specifically at the stenosed region. The concentration of stenosis-induced flow changes in the narrowed section leads to increased strain and deformation of the arterial wall, particularly in the stenosed area. Both figures demonstrate a bending effect, with an interesting observation regarding the relative bending in 70% and 90% stenosed conditions at the femoral artery.

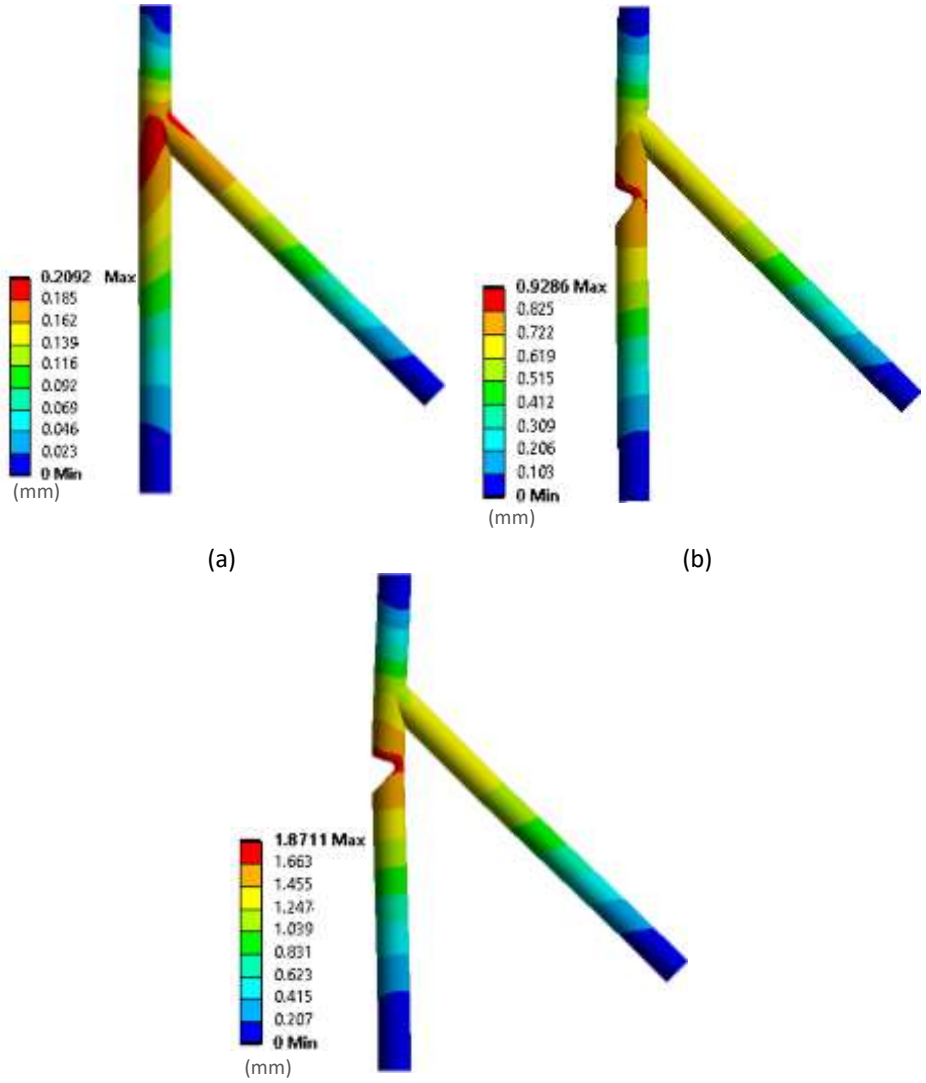

Fig. 9. Total deformation contours (mm) (a) normal artery, (b) 70% blockage, and (c) 90% blockage

3.5 Limitation

Despite the valuable insights gained from this study, it is important to acknowledge certain limitations. primarily related to the geometric representation and the one-way FSI approach employed. Firstly, the idealized nature of the CFA model, though constructed based on clinical data, may not fully capture the anatomical intricacies and variations present in real-world patient cases. Patient-specific geometries could provide a more accurate representation but may introduce complexities that are challenging to address comprehensively. Additionally, the one-way FSI method used in this study assumes a rigid arterial wall, neglecting the potential feedback effect where arterial wall deformation influences blood flow. This simplification might limit the study's ability to capture dynamic interactions between blood and arterial wall behavior accurately. Future investigations incorporating more realistic geometries and employing fully coupled FSI methods could offer a more detailed and physiologically relevant exploration of peripheral arterial dynamics.

4. Conclusions

In conclusion, this research project focused on the development of a FSI model to predict potential atherosclerosis locations in healthy and stenosed peripheral arteries, specifically at 70% and 90% stenosis levels. The study utilized an idealized model of the CFA with trapezium-type stenosis, incorporating CFD and finite element-based simulations. The results provided valuable insights into the complex interplay between hemodynamics and arterial wall mechanics.

The velocity contours illustrated distinct flow patterns in normal, 70% stenosed, and 90% stenosed arteries, revealing the impact of varying degrees of stenosis on blood flow dynamics. The maximum outlet velocity demonstrated adaptive hemodynamics in response to stenosis, with reduced flow in the stenosed artery compensated by increased velocity in PFA. These findings have significant clinical implications for risk assessment and treatment planning in arterial diseases.

WSS contours highlighted regions of low WSS, particularly after bifurcation and around the stenosed area, indicating susceptibility to plaque formation. The drastic reduction in WSS along SFA in the 90% stenosed artery underscored the critical nature of severe stenosis, emphasizing the potential for adverse clinical outcomes.

Pressure shows the linear decline in pressure along the normal artery due to bifurcation and reflects uniform losses from viscous shear, a characteristic feature of unobstructed flow. However, the introduction of stenosis has profoundly altered the pressure profiles.

Total deformation analysis revealed a progressive increase in arterial wall deformation with higher degrees of stenosis. The concentration of deformation at the stenosed area indicated the localized impact of stenosis on fluid dynamics and wall stresses, with implications for plaque formation and potential rupture.

While the study provided valuable insights into the complexities of hemodynamics and arterial wall mechanics in PAD, future work should focus on the comparison and validation of computational predictions with clinical follow-up data. Additionally, further exploration of fully coupled FSI models and consideration of patient-specific geometries could enhance the clinical relevance of the findings.

Acknowledgement

The authors would like to thank the Ministry of Higher Education for providing financial support under Fundamental Research Grant Scheme (FRGS) No.FRGS/1/2021/TK0/UMP/02/8 (University reference RDU210109)).

References

[1] Eberhardt, Robert. "100 Questions & Answers About Peripheral Arterial Disease (PAD) by Emile Mohler III and Alan T Hirsch eds." *Vascular Medicine (London, England)* (2010).

[2] Horváth, Lilla, Noémi Németh, Gergely Fehér, Zsuzsanna Kívés, Dóra Endrei, and Imre Boncz. "Epidemiology of peripheral artery disease: narrative review." *Life* 12, no. 7 (2022): 1041. https://doi.org/10.3390/life12071041

[3] Criqui, Michael H., and Victor Aboyans. "Epidemiology of peripheral artery disease." *Circulation Research* 116, no. 9 (2015): 1509-1526. https://doi.org/10.1161/CIRCRESAHA.116.303849

[4] Galizia, Mauricio S., Alex Barker, Yihua Liao, Jeremy Collins, James Carr, Mary M. McDermott, and Michael Markl. "Wall morphology, blood flow and wall shear stress: MR findings in patients with peripheral artery disease." *European Radiology* 24 (2014): 850-856. https://doi.org/10.1007/s00330-013-3081-x

[5] Papathanasopoulou, Panorea, Shunzhi Zhao, Uwe Köhler, Malcolm B. Robertson, Quan Long, Peter Hoskins, X. Yun Xu, and Ian Marshall. "MRI measurement of time-resolved wall shear stress vectors in a carotid bifurcation model, and comparison with CFD predictions." *Journal of Magnetic Resonance Imaging* 17, no. 2 (2003): 153-162. https://doi.org/10.1002/jmri.10243

[6] Cibis, Merih, Wouter V. Potters, Mariana Selwaness, Frank J. Gijsen, Oscar H. Franco, Andres M. Arias Lorza, Marleen de Bruijne et al. "Relation between wall shear stress and carotid artery wall thickening MRI versus CFD." *Journal of Biomechanics* 49, no. 5 (2016): 735-741. https://doi.org/10.1016/j.jbiomech.2016.02.004

[7] Shahrulakmar, Ukasyah Zulfaqar, Nasrul Hadi Johari, Muhammad Firdaus Mohd Fauzi, Juhara Haron, Chandran Nadarajan, and Mohd Nadzeri Omar. "Numerical Approach for The Evaluation of Hemodynamic Behaviour in Peripheral Arterial Disease: A Systematic Review." *Journal of Advanced Research in Fluid Mechanics and Thermal Sciences* 103, no. 2 (2023): 95-117. https://doi.org/10.37934/arfmts.103.2.95117

[8] Shahrulakmar, U. Z., M. N. Omar, and N. H. Johari. "Brief review on recent advancement of computational analysis on hemodynamics in peripheral artery disease." In *International Conference on Mechanical Engineering Research*, pp. 555-572. Singapore: Springer Nature Singapore, 2021. https://doi.org/10.1007/978-981-19-1577-2_41

[9] Lopes, D., Hélder Puga, J. Carlos Teixeira, and S. F. Teixeira. "Influence of arterial mechanical properties on carotid blood flow: Comparison of CFD and FSI studies." *International Journal of Mechanical Sciences* 160 (2019): 209-218. https://doi.org/10.1016/j.ijmecsci.2019.06.029

[10] Johari, Nasrul Hadi, M. Hamady, and Xiao Yun Xu. "Fluid-Structure Interaction Study of The Effect of Stent on Local Hemodynamics Parameters at The Stented Carotid Artery Bifurcation." *Journal of Advanced Research in Applied Sciences and Engineering Technology* 28, no. 2 (2022): 247-255. https://doi.org/10.37934/araset.28.2.247255

[11] Schoenborn, Sabrina, Selene Pirola, Maria A. Woodruff, and Mark C. Allenby. "Fluid-structure interaction within models of patient-specific arteries: computational simulations and experimental validations." *IEEE Reviews in Biomedical Engineering* 17 (2022): 280-296. https://doi.org/10.1109/RBME.2022.3215678

[12] Chen, Xueping, Jian Zhuang, Huanlei Huang, and Yueheng Wu. "Fluid-structure interactions (FSI) based study of low-density lipoproteins (LDL) uptake in the left coronary artery." *Scientific Reports* 11, no. 1 (2021): 4803. https://doi.org/10.1038/s41598-021-84155-3

[13] Javadzadegan, Ashkan, Azadeh Lotfi, Anne Simmons, and Tracie Barber. "Haemodynamic analysis of femoral artery bifurcation models under different physiological flow waveforms." *Computer Methods in Biomechanics and Biomedical Engineering* 19, no. 11 (2016): 1143-1153. https://doi.org/10.1080/10255842.2015.1113406

[14] Wang, Danyang, Ferdinand Serracino-Inglott, and Jiling Feng. "Numerical simulations of patient-specific models with multiple plaques in human peripheral artery: a fluid-structure interaction analysis." *Biomechanics and Modeling in Mechanobiology* 20, no. 1 (2021): 255-265. https://doi.org/10.1007/s10237-020-01381-w

[15] Kim, Young-Ho, Jong-Eun Kim, Yasushi Ito, Alan M. Shih, Brigitta Brott, and Andreas Anayiotos. "Hemodynamic analysis of a compliant femoral artery bifurcation model using a fluid structure interaction framework." *Annals of Biomedical Engineering* 36 (2008): 1753-1763. https://doi.org/10.1007/s10439-008-9558-0

[16] Gökgöl, Can, Yasushi Ueki, Daniel Abler, Nicolas Diehm, Rolf P. Engelberger, Tatsuhiko Otsuka, Lorenz Räber, and Philippe Büchler. "Towards a better understanding of the posttreatment hemodynamic behaviors in femoropopliteal arteries through personalized computational models based on OCT images." *Scientific Reports* 11, no. 1 (2021): 16633. https://doi.org/10.1038/s41598-021-96030-2

[17] Smilde, Tineke J., Franchette W. P. J. van den Berkmortel, Godfried H. J. Boers, Hub Wollersheim, Theo de Boo, Herman van Langen, and Anton F. H. Stalenhoef. "Carotid and femoral artery wall thickness and stiffness in patients at risk for cardiovascular disease, with special emphasis on hyperhomocysteinemia." *Arteriosclerosis, Thrombosis, and Vascular Biology* 18, no. 12 (1998): 1958-1963. https://doi.org/10.1161/01.ATV.18.12.1958

[18] Choi, Gilwoo, Christopher P. Cheng, Nathan M. Wilson, and Charles A. Taylor. "Methods for quantifying three-dimensional deformation of arteries due to pulsatile and nonpulsatile forces: implications for the design of stents and stent grafts." *Annals of Biomedical Engineering* 37 (2009): 14-33. https://doi.org/10.1007/s10439-008-9590-0

[19] Wood, Nigel B., Shun Z. Zhao, Andrew Zambanini, Mark Jackson, W. Gedroyc, Simon A. Thom, Alun D. Hughes, and Xiao Yun Xu. "Curvature and tortuosity of the superficial femoral artery: a possible risk factor for peripheral arterial disease." *Journal of Applied Physiology* 101, no. 5 (2006): 1412-1418. https://doi.org/10.1152/japplphysiol.00051.2006

[20] Lorenzini, Giulio, and Erminio Casalena. "CFD analysis of pulsatile blood flow in an atherosclerotic human artery with eccentric plaques." *Journal of Biomechanics* 41, no. 9 (2008): 1862-1870. https://doi.org/10.1016/j.jbiomech.2008.04.009

[21] Moser, K. W., E. C. Kutter, J. G. Georgiadis, R. O. Buckius, H. D. Morris, and J. R. Torczynski. "Velocity measurements of flow through a step stenosis using Magnetic Resonance Imaging." *Experiments in Fluids* 29, no. 5 (2000): 438-447. https://doi.org/10.1007/s003480000110

[22] Kamangar, Sarfaraz, Irfan Anjum Badruddin, N. Ameer Ahamad, Kalimuthu Govindaraju, N. Nik-Ghazali, N. J. Ahmed, A. Badarudin, and T. M. Khan. "The influence of geometrical shapes of stenosis on the blood flow in stenosed artery." *Sains Malaysiana* 46, no. 10 (2017): 1923-1933. https://doi.org/10.17576/jsm-2017-4610-31

[23] Lee, Minhyung, Gwanyong Park, Changyoung Park, and Changmin Kim. "Improvement of grid independence test for computational fluid dynamics model of building based on grid resolution." *Advances in Civil Engineering* 2020, no. 1 (2020): 8827936. https://doi.org/10.1155/2020/8827936

[24] Quemada, D. J. R. A. "Rheology of concentrated disperse systems II. A model for non-newtonian shear viscosity in steady flows." *Rheologica Acta* 17, no. 6 (1978): 632-642. https://doi.org/10.1007/BF01522036

[25] Razhali, Nur Farahalya, and Ishkrizat Taib. "Analysis of Hemodynamic on Different Stent Strut Configurations in Femoral Popliteal Artery." *CFD Letters* 14, no. 3 (2022): 119-128. https://doi.org/10.37934/cfdl.14.3.119128
[26] Widiawaty, Candra Damis, Ahmad Indra Siswantara, Muhammad Arif Budiyanto, Mohammad Arif Andira, Dendy Adanta, Muhammad Hilman Gumelar Syafe'i, Tanwir Ahmad Farhan, and Illa Rizianiza. "Analysis of Mesh Resolution Effect to Numerical Result of CFD-ROM: Turbulent Flow in Stationary Parallel Plate." *CFD Letters* 16, no. 8 (2024): 1-17. https://doi.org/10.37934/cfdl.16.8.117
[27] Lopes, D., Hélder Puga, J. Teixeira, and R. Lima. "Blood flow simulations in patient-specific geometries of the carotid artery: A systematic review." *Journal of Biomechanics* 111 (2020): 110019. https://doi.org/10.1016/j.jbiomech.2020.110019
[28] Langtry, Robin B., and Florian R. Menter. "Correlation-based transition modeling for unstructured parallelized computational fluid dynamics codes." *AIAA Journal* 47, no. 12 (2009): 2894-2906. https://doi.org/10.2514/1.42362
[29] Menter, Florian R. "Two-equation eddy-viscosity turbulence models for engineering applications." *AIAA Journal* 32, no. 8 (1994): 1598-1605. https://doi.org/10.2514/3.12149
[30] Abd Halim, M. A., N. A. R. Nik Mohd, M. N. Mohd Nasir, and M. N. Dahalan. "The evaluation of k-ε and k-ω turbulence models in modelling flows and performance of s-shaped diffuser." *International Journal of Automotive and Mechanical Engineering* 15, no. 2 (2018): 5161-5177. https://doi.org/10.15282/ijame.15.2.2018.2.0399
[31] Saad, Idris, and S. Bari. "CFD investigation of in-cylinder air flow to optimize number of guide vanes to improve ci engine performance using higher viscous fuel." *International Journal of Automotive and Mechanical Engineering* 8 (2013): 1096-1107. https://doi.org/10.15282/ijame.8.2013.1.0089
[32] Johari, Nasrul Hadi, Mohamad Hamady, and Xiao Yun Xu. "A computational study of the effect of stent design on local hemodynamic factors at the carotid artery bifurcation." *Artery Research* 26, no. 3 (2020): 161-169. https://doi.org/10.2991/artres.k.200603.001
[33] Tan, F. P. P., G. Soloperto, S. Bashford, N. B. Wood, S. Thom, A. Hughes, and X. Y. Xu. "Analysis of flow disturbance in a stenosed carotid artery bifurcation using two-equation transitional and turbulence models." *Journal of Biomechanical Engineering* 130, no. 6 (2008): 061008. https://doi.org/10.1115/1.2978992
[34] Hutchinson, B. R., and G. D. Raithby. "A multigrid method based on the additive correction strategy." *Numerical Heat Transfer, Part A: Applications* 9, no. 5 (1986): 511-537. https://doi.org/10.1080/10407788608913491
[35] Colombo, Monika, Marco Bologna, Marc Garbey, Scott Berceli, Yong He, Josè Felix Rodriguez Matas, Francesco Migliavacca, and Claudio Chiastra. "Computing patient-specific hemodynamics in stented femoral artery models obtained from computed tomography using a validated 3D reconstruction method." *Medical Engineering & Physics* 75 (2020): 23-35. https://doi.org/10.1016/j.medengphy.2019.10.005
[36] Prendergast, P. J., C. Lally, S. Daly, A. J. Reid, T. C. Lee, D. Quinn, and F. Dolan. "Analysis of prolapse in cardiovascular stents: a constitutive equation for vascular tissue and finite-element modelling." *Journal of Biomechanical Engineering* 125, no. 5 (2003): 692-699. https://doi.org/10.1115/1.1613674
[37] Tang, Dalin, Chun Yang, Shunichi Kobayashi, Jie Zheng, and Raymond P. Vito. "Effect of stenosis asymmetry on blood flow and artery compression: a three-dimensional fluid-structure interaction model." *Annals of Biomedical Engineering* 31 (2003): 1182-1193. https://doi.org/10.1114/1.1615577
[38] Gupta, Prashant, Shannon Lyons, and Sandeep Hedgire. "Ultrasound imaging of the arterial system." *Cardiovascular Diagnosis and Therapy* 9, no. Suppl 1 (2019): S2. https://doi.org/10.21037/cdt.2019.02.05
[39] Malek, Adel M., Seth L. Alper, and Seigo Izumo. "Hemodynamic shear stress and its role in atherosclerosis." *JAMA* 282, no. 21 (1999): 2035-2042. https://doi.org/10.1001/jama.282.21.2035
[40] Amdilah, Nur Syuhada Che, Yu Shi Lau, Yih Miin Liew, W. N. W. Ab Naim, and Mohd Jamil Mohamed Mokhtarudin. "Computational fluid dynamics of patient-specific coronary artery during stent treatment." In *Engineering Technology International Conference (ETIC 2022)*, vol. 2022, pp. 216-220. IET, 2022. https://doi.org/10.1049/icp.2022.2608
[41] Teng, Zhongzhao, Adam J. Brown, Patrick A. Calvert, Richard A. Parker, Daniel R. Obaid, Yuan Huang, Stephen P. Hoole, Nick EJ West, Jonathan H. Gillard, and Martin R. Bennett. "Coronary plaque structural stress is associated with plaque composition and subtype and higher in acute coronary syndrome: the BEACON I (Biomechanical Evaluation of Atheromatous Coronary Arteries) study." *Circulation: Cardiovascular Imaging* 7, no. 3 (2014): 461-470. https://doi.org/10.1161/CIRCIMAGING.113.001526
[42] Tang, Dalin, Chun Yang, Jie Zheng, Pamela K. Woodard, Kristen Billiar, Zhongzhao Teng, and Richard Bach. "3D in vivo IVUS-based anisotropic FSI models with cyclic bending for human coronary atherosclerotic plaque mechanical analysis." In *Summer Bioengineering Conference*, vol. 48913, pp. 181-182. American Society of Mechanical Engineers, 2009. https://doi.org/10.1115/SBC2009-204700
[43] Johari, Nasrul Hadi, Jegatis Balaiyah, and Zulkifli Ahmad. "Effect of chronic obstructive pulmonary disease on airflow motion using computational fluid dynamics analysis." In *2014 International Conference on Computer, Communications, and Control Technology (I4CT)*, pp. 249-254. IEEE, 2014.

https://doi.org/10.1109/I4CT.2014.6914184

[44] Johari, Nasrul Hadi, Kahar Osman, Zuliaazura Mohd Salleh, Juhara Haron, and Mohammed Rafiq Abdul Kadir. "The effect of different locations of tracheal stenosis to the flow characteristics using reconstructed CT-scanned image." *Journal of Mechanics in Medicine and Biology* 12, no. 04 (2012): 1250066. https://doi.org/10.1142/S0219519412500662